

Essential Principles and Practices in X-ray Photoelectron Spectroscopy

Jan Čechal*

CEITEC and Institute of Physical Engineering,
Brno University of Technology, Brno, Czech Republic.

(Dated: January 1, 2026)

X-ray Photoelectron Spectroscopy (XPS) is a widely utilized technique for chemical analysis of solid surfaces, sensitive to the chemical environment of atoms via core-level binding energy shifts. While modern instruments allow obtaining the experimental data with ease, their evaluation and interpretation is challenging to newcomers to the field as a profound knowledge of the method is required for a correct analysis. Here we present a concise yet comprehensive introduction to the fundamental principles and methodologies of XPS, covering photoemission processes, chemical shifts, charge referencing, peak fitting, and quantification strategies. This overview aims to bridge the gap between data collection and reliable analysis, providing essential knowledge for correct interpretation. By clarifying key concepts and common practices, this work supports improved accuracy in surface chemical characterization using XPS.

Keywords: X-ray Photoelectron Spectroscopy, XPS, ESCA

I. INTRODUCTION

X-ray photoelectron spectroscopy (XPS) is a method for chemical analysis of near-surface layers of materials. Its primary advantage is its sensitivity to the chemical environment of probed atoms as revealed by shifts in binding energies (BE) of core levels. In recent years, the widespread adoption of this method has been accompanied by a high rate of incorrect analyses and interpretations, reaching as much as 60 % [1], which has been identified as a pre-crisis situation [2]. Addressing this issue through improved education and awareness is essential to prevent a full-blown crisis in the field [2]. While many resources are available — including the well-known “red” [3] and “blue” [4] books on XPS, reviews [5, 6], series of tutorial papers [7], and a guideline to avoid the common errors [8] — these are often lengthy and not easily accessible for quick reference. In this work, we provide a brief yet comprehensive introduction to XPS; serving as a signpost to guide readers to the source of knowledge they may need. To maintain conciseness, we do not discuss exceptions to general rules that are valid in more than 90 % of cases; such exceptions are marked with “(! 23)”, where the number refers to a note in Appendix A.

II. PHOTOELECTRON SPECTRUM

Process of photoemission. In XPS, a vacuum compatible sample is irradiated by monochromatic Al K α X-rays (! 1) of energy $E_{\text{Al K}\alpha} = 1486.6 \text{ eV}$ (Fig. 1A). The radiation penetrates a few micrometers to the sample (Fig. 1B), where it can be absorbed by an atom, which subsequently emits a photoelectron from a core level with binding energy of E_{CL} (Fig. 1C). The kinetic energy of photoelectron is E_{kin}^* . The energy distribution of measured electron kinetic energies E_{kin} is referred to as a photoelectron spectrum (Fig. 1D). We consider photoemis-

sion, photoelectron transport through a solid, and escape through the surface to vacuum as independent events. The spectrum also contains contributions from other processes, such as X-ray-induced Auger electrons or inelastically scattered electrons that form a background. Due to inelastic scattering during transport in a solid, only electrons emitted within the topmost few nanometers of the sample can escape and be detected (Fig. 1B) [5, 9].

Energy conservation relates the measured kinetic energies electrons with BE of core levels from which they were emitted (Fig. 1E). BEs are referenced typically to sample Fermi level $E_{\text{CL}}^{\text{B}, \text{F}}$ or more rarely to vacuum level $E_{\text{CL}}^{\text{B}, \text{V}}$; these energy levels are mutually shifted by sample work function φ_{sample} : $E_{\text{CL}}^{\text{B}, \text{V}} = E_{\text{CL}}^{\text{B}, \text{F}} + \varphi_{\text{sample}}$. For *conductive* samples, the common Fermi level is established between the sample and the spectrometer by grounding of both; then, the energy conservation relation is

$$E_{\text{kin}} = E_{\text{Al K}\alpha} - E_{\text{CL}}^{\text{B}, \text{F}} - \varphi_{\text{spectrometer}}, \quad (1)$$

featuring a constant spectrometer work function $\varphi_{\text{spectrometer}}$ (Fig. 1E) [10]. Hence, for grounded conductive samples, the measured BEs are independent on φ_{sample} , making the Fermi level referencing general approach for a variety of samples. Equation (1) is used for the conversion of the axis of kinetic energies to the axis of binding energies; it is a convention to plot the binding energy axis with BE increasing to the left. For *non-conductive* (insulating) samples or physisorbed species, the common Fermi level is not established, and equation (1) is no longer valid, it is replaced by

$$E_{\text{kin}} = E_{\text{Al K}\alpha} - E_{\text{CL}}^{\text{B}, \text{F}} - \varphi_{\text{sample}} + V, \quad (2)$$

where V is an external potential due to, e.g., employed charge neutralization [10]. Insulating samples would charge positively due to emission of electrons; to prevent the charging, samples are supplied by low-energy electrons from vacuum side (! 2), which is referred to as charge neutralization [11, 12]. We note that charge neutralization is not perfect, and artifacts can arise from differential charging.

* cechal@fme.vutbr.cz

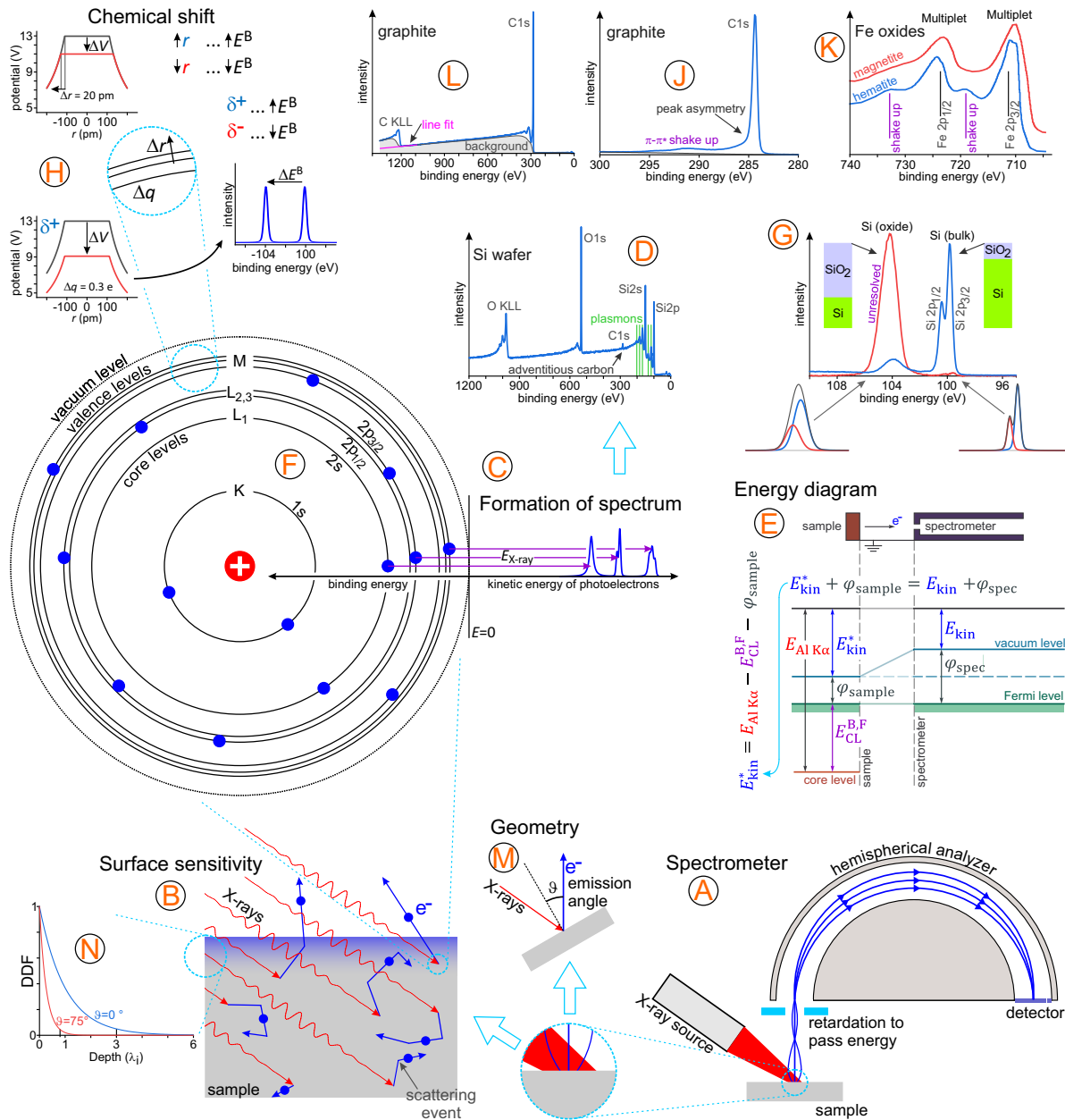


Figure 1. Summary of XPS. (A) Typical experimental setup. (B) X-rays penetrate μm into the sample, whereas the electrons can escape only from a few nm according to the depth distribution function (DDF) given in (N) for two distinct emission angles defined in (M). (C) Formation of the spectrum by excitation of electrons with radiation of constant energy of $E_{\text{X-ray}}$. (D) Photoelectron spectrum of Si wafer; vertical lines highlight plasmon loss peaks. (E) Energy diagram defining energy conservation rules. Eq. (1) is obtained by combining energy conservation for sample-spectrometer contact and photoemission events. (F) Schematics of the probed atom with marking of inner shells in X-ray and spectroscopic notations. (G) Detailed Si 2p spectra of two distinct thicknesses of oxide layer on bulk Si. Both peaks are doublets; their fitting is detailed in the bottom part. (H) Charged shell model for chemical shifts. Changing either valence charge density by Δq of the mean radius of the valence level $\langle r \rangle$ changes the inner potential within the shell, which changes the BE of electrons on core levels. The potential is given as a function of $\langle r \rangle$; inside the shell, the potential is constant. (J) Detailed C 1s spectrum of graphite showing its inherent asymmetry and shake-up satellite. (K) Detailed Fe 2p spectra of pure Fe oxides (magnetite and hematite) showing broad peaks of complicated shape due to multiplet splitting. (L) Photoelectron spectrum of graphite showing with marked background and straight line fit of C KLL.

Core levels. If an atom of given element is present in the probed volume, all its accessible core-level peaks are observed with given relative intensities; the sensitivity is $\sim 0.1\text{--}1$ atomic % [13]. The BEs of core-levels, obtained from equation (1), depend on chemical state of the atom, such as bonding

to other atoms or their position within the crystal lattice. Peaks associated with core-levels are labeled according to the quantum numbers of the level from which the electron was emitted (Fig. 1F). For example, $2p_{3/2}$ refers to emission from level with principal number $n = 2$, azimuthal number $l = 1$ (labeled as

s, p, d, and f for $l=0, 1, 2$, and 3 , respectively), and the total angular momentum number $j=3/2$, where j is the sum of orbital and spin angular momenta ($l \pm \frac{1}{2}$). Levels with $l=1$ (p), 2 (d), or 3 (f) are split by spin-orbit coupling into two components with a different j values (Fig. 1G); these components have characteristic energy separations and intensity ratios (!3) of 1:2, 2:3 or 3:4 for p, d, and f levels, respectively [5, 13]. Both components represent the same chemical state.

Chemical shifts. The chemical (BE) shifts provide a direct way to characterize the chemical environment of the probed atoms. The relationship between the chemical state and the measured BE position of the peak is not unique: distinct chemical states can result in the same BE. We distinguish between initial state effects, which occur before the photoemission event, and final state effects, which occur as a response to photoemission [14, 15]. Both types of effects depend on the valence charge density and its distribution (!4). The initial state effect can be illustrated (Fig. 1H) by modeling the valence electrons as a thin spherical shell of mean radius $\langle r \rangle$ carrying charge q [3, 14]. The potential inside this shell is constant and proportional to $\frac{q}{\langle r \rangle}$; this potential reduces the effective potential experienced by the core-level electrons, thereby affecting their binding energy. Increasing the valence charge density or decreasing the mean radius lowers the BE while decreasing the charge density or increasing the radius raises the BE. Final state effects involve the response of the atom to formation of core hole, mainly through screening by valence electrons [14]. It is important to note that oxygen vacancies are not detectable in the O 1s spectrum, as there is no photoemission from a missing atom and the next-nearest-neighbor effects are also not present [16, 17].

Charge referencing. For insulating samples, establishing correct values of BE is challenging [10]; equation (2) must be used, and the spectrum is shifted with an unknown value of V . A commonly used approach is to shift the spectrum so that position of C 1s of adventitious carbon (AdC, Fig. 1D) appears at 284.8 eV (!5) [18]. However, since the AdC aligns with vacuum level [19], equation (1) does not apply, making this approach fundamentally flawed [10]. Nevertheless, it remains widely used due to a lack of simple alternatives [10].

Peak fitting. The primary goal in XPS is to identify chemical environments (e.g., bonding) of atoms in the sample from the position of the peaks, using reference values of chemical shifts. When multiple chemical environments are present, measured peaks may have complex shapes that are typically decomposed by modeling them by synthetic components (Fig. 1G); this procedure is referred to as peak fitting [20, 21]. The spectrum is fitted by set of peaks described by Voigt functions, which are convolutions of Lorentzian and Gaussian functions [8, 22]. The Lorentzian component is associated with the photoemission process, and its width is proportional to core-hole lifetime [5, 23]. The Gaussian component

reflects instrumental broadening or broadening due to variations in the chemical environment, such as in amorphous oxides (Fig. 1G) [5]. For inherently asymmetric peaks the Lorentzian is replaced by Doniach-Sunjic function [5, 24]. Spin-orbit split components are modeled as doublet peaks (doublets) with given energy separation and intensity ratio (see above); both components represent a single chemical environment. It should be noted that not every spectrum requires fitting; in many cases, the necessary information can be obtained without it.

III. OTHER FEATURES IN PHOTOELECTRON SPECTRUM

The photoelectron spectrum contains wealth of information; experimentalists are encouraged to utilize the full spectra, not just core-level peaks.

Shake-up satellite peaks arise due to electron excitation accompanying the photoemission process, leading to a characteristic loss of energy [4]. The presence or absence of these satellites is indicative for specific chemical environments [25]; for example, presence of $\pi - \pi^*$ satellite (Fig. 1J) for aromatic systems [26]. Intensity of shake-up satellites should be included in quantification (!6) [27]. A similar effect, involving the excitation of electron in the conduction band near the Fermi level leads to inherent asymmetry of peaks (Fig. 1J) associated with many conductors [5].

Multiplet splitting. Photoemission from certain atoms, particularly transition metal atoms in paramagnetic states, can result in multiple peaks associated with a single chemical state due to coupling of high angular momentum of atom with angular momentum of created core-hole [14, 28]. For example, both hematite and magnetite (Fig. 1K) should be represented with multiple (more than four) overlapping peaks, rather than a single component, to accurately reflect their multiplet splitting [29].

Auger peaks. The relaxation of atoms left with a core hole after photoemission can proceed via the Auger process. A series of Auger peaks (Fig. 1D, L) is a typical feature found in the XPS spectra [3]. Auger peaks provide additional information beyond that of the core-levels, especially when the kinetic energy of Auger peak E_{AE} is combined with binding energy of core level $E_{CL}^{B,F}$ of the same element to form a modified Auger parameter $\alpha^* = E_{CL}^{B,F} + E_{AE}$; the values of α^* enable chemical speciation in cases where chemical shifts alone are insufficient [30, 31]. In some cases, the visual inspection of the Auger peak shape and its comparison with reference spectra can provide the necessary information about the chemical environment of studied atoms.

Extrinsic effects. The additional features arise during the electron transport through solid. For example, inelastic scattering of photoelectrons gives rise to background signals (Fig. 1L) [32] while the excitation of plasmons leads to series of loss peaks (Fig. 1D) [13]. These plasmon loss peaks are charac-

teristic by their constant energy separation and decreasing intensity with increasing binding energies.

IV. PHOTOELECTRON TRANSPORT THROUGH A SOLID

Depth distribution function [33]. The probability that a photoelectron originating at depth z escapes the sample at emission angle ϑ (Fig. 1M) is given by (!7) [6, 33]

$$\phi(z, \vartheta) = e^{\left(\frac{z}{\lambda_i \cos \vartheta}\right)}, \quad (3)$$

that is, the signal decays exponentially with depth (Fig. 1N), with a characteristic length determined by the inelastic mean free path λ_i [9]. λ_i depends on the material and kinetic energy of electron E_{kin}^* .

Background. The longer the path that electrons travel the greater the extent of inelastic scattering. Inelastically scattered electrons contribute to the background on the higher BE side of the peak. Backgrounds therefore carry information on the depth distribution of elements in the sample [32]. For peak fitting and quantification, the background must be subtracted. This is typically done by first removing the pre-peak background using a straight line fit (Fig. 1L) followed by applying an appropriate background function, such as Shirley or Tougaard function (Fig. 1L) [32, 34].

Elastic Scattering. Electrons can be also scattered elastically, meaning their direction of propagation changes while their energy remains unchanged; this affects the quantification and determination of layer thickness described below; for emission angles $\vartheta > 60^\circ$ elastic scattering cannot be neglected [9]. To account for elastic scattering, the inelastic mean free path λ_i is replaced by the effective attenuation length (EAL) λ_A [9].

V. QUANTIFICATION

Homogeneous samples. For a calibrated instrument (!8) and the given density of incident X-rays $I_{\text{X-ray}}$, the photoelectron intensity of peak (peak area) of core level CL of element A measured at the emission angle ϑ is given by [3]

$$I_{\text{CL}} = I_{\text{X-ray}} \sigma_{\text{CL}} L_{\text{CL}} \int_{z=0}^{\infty} n_A(z) \phi(z, \vartheta) dz. \quad (4)$$

This intensity is proportional to depth distribution of concentration $n_A(z)$ of element A in the sample and photoemission cross section σ_{CL} of CL of A; the angular photoemission asymmetry term L_{CL} is the same for all elements and lines if the spectrometer is the “magic angle geometry” (!9). Assuming a homogenous distribution of all elements in the sample $n_A(z) = \text{const}$, and removing the terms that are the same for all elements, we obtain set of relative intensities $I_{\text{CL}}^{\text{homogeneous}} = n_A \lambda_i$, which are subsequently

rearranged and normalized over all elements to yield the relative atomic concentrations [6]

$$n_A^{\text{rel}} = \frac{\frac{I_{\text{CL}}}{\sigma_{\text{CL}} \lambda_i}}{\sum_{\text{all elements}} \frac{I_{\text{CL}}}{\sigma_{\text{CL}} \lambda_i}}. \quad (5)$$

The term $\sigma_{\text{CL}} \lambda_i$ is often referred to as sensitivity factor. While the process is straightforward, several critical considerations are necessary to obtain accurate information [35]; typically, the absolute precision is 4–15 % [27] but the changes down to 1 % can be detected between the samples [35]. Equation (5) is provided by most software tools, but the validity of the crucial assumption of a homogeneous sample remain the responsibility of the researchers.

Inhomogeneous samples. Equation (4) can be used to derive the formulas for determining layer thickness [9]. Considerable effort has been devoted to developing methodologies for determining the depth distribution of elements $n_A(z)$ in the sample from a series of spectra taken at distinct angles [36], but this never resulted in a universal tool.

When XPS is combined with an ion beam, a depth profile of elements can be obtained [37], however, since the ion beam alters most of the probed volume, information about the chemical environment is typically lost [5].

VI. CONCLUSIONS

X-ray photoelectron spectroscopy can be used to obtain quantitative information about the elements in a sample and to determine their chemical environments. Analyses must adhere to physical principles while considering the sample chemistry. The primary virtue of XPS analysis is consistency. First, there should be consistency across the spectrum: all peaks associated with the element should appear with relative intensities as expected from theory (proportional to sensitivity factors $\sigma_{\text{CL}} \lambda_i$). Second, there should be consistency across the chemical states: for example, if bonding between carbon and nitrogen is identified in the C 1s spectrum with intensity $\propto \sigma_{\text{C 1s}} \lambda_i$, the corresponding nitrogen bonding should be present in the N 1s spectrum with a matching intensity ($\propto \sigma_{\text{N 1s}} \lambda_i$). Third, consistency should be maintained across the series of samples: similar approaches, such as background subtraction or peak fitting, should be applied to all the samples unless a clear justification is provided for any differences. Several critical points for correct analysis and interpretation that are often overlooked [5, 8]: (i) it is not necessary to fit all spectra (ii) peak fitting must follow strict rules; (iii) often, two or more peaks are associated with a single chemical state: p, d, and f peaks are spin-orbit split doublets and transition metals exhibit complex peak shapes due to multiplet splitting; (iv) quantitative analysis assumes a homogeneous sample; and (v) incorrect practices present in the literature should not be repeated.

ACKNOWLEDGMENTS

We thank Brno University of Technology for support through the Excellence Research Fund.

Appendix A: Notes to general rule exceptions

1. Monochromatic Al K α X-ray source is standard equipment in modern instruments. However, many instruments are still equipped with a non-monochromatic Mg/Al dual X-ray source. In the X-ray spectrum of such sources, a single K $\alpha_{1,2}$ line is dominant, but weaker lines such as K $\alpha_{3,4}$ and K β are also present; these additional lines also excite photoelectrons, resulting in non-monochromatic satellite features that appear at the lower BE side of the peaks exited with the main X-ray line [13]. Dual anode sources offer two distinct X-ray energies, which can be used to distinction of Auger peaks from photoelectron peaks.

Alternatively, synchrotron radiation can be used as an X-ray source, offering superior energy resolution and enabling advanced techniques beyond standard XPS. When using polarized X-rays with tunable energy, several parameters change: for example, photoionization cross sections become energy dependent, and both the angular asymmetry parameter [35] and effective attenuation lengths (EALs) [9] differ compared to unpolarized laboratory sources.

2. The exit part of the dual anode X-ray source, which consists of an aluminum window positioned close to the sample, generates a significant number of stray electrons [13]. When sample charging occurs, these electrons are attracted to the sample and partially neutralize it. As a result, the measured

spectrum is shifted by up to ~ 10 eV towards higher BEs.

- 3.** Photoemission is a quantum mechanical process, which sometimes results in slightly different separations and intensity ratios than those predicted by the state multicity rule [8]. The example can be the broadening of Ti 2p_{1/2} [38]. It should be noted that although the higher BE component of the doublet may experience slight broadening [20], the intensity ratio (given by the peak areas) remains at those predicted by the state multicity rule.
- 4.** Because photoemission is an inherently quantum mechanical effect, simplified models may not account for all observed phenomena [14].
- 5.** Sometimes the value of 285.0 is used [18].
- 6.** When using theoretical sensitivity factors [27]. See point 8.
- 7.** Depth distribution function in the simplest expression – a straight-line approximation, neglecting the elastic scattering [33].
- 8.** Instrument calibrated for the transmission function. Some instruments are calibrated with respect to a “true spectrum” (a reference spectrum provided by NIST); in this case, theoretical sensitivity factors can be used for quantification [35]. However, some instruments are calibrated to the manufacturer’s reference; in this case, instrument-bound sensitivity factors should be used. Other Spectrometer calibrations include those for binding energies [13] and detector linearity [5, 35].
- 9.** If the angle between the X-ray source and spectrometer is 54.7°, the angular asymmetry is the same for all lines and elements [3].
- 23.** This is an example of a reference given in the introduction.

[1] G. H. Major, T. G. Avval, B. Moeini, G. Pinto, D. Shah, V. Jain, V. Carver, W. Skinner, T. R. Gengenbach, C. D. Easton, A. Herrera-Gomez, T. S. Nunney, D. R. Baer, and M. R. Linford, Assessment of the frequency and nature of erroneous x-ray photoelectron spectroscopy analyses in the scientific literature, *Journal of Vacuum Science & Technology A* **38**, 061204 (2020).

[2] G. H. Major, J. W. Pinder, D. E. Austin, D. R. Baer, S. L. Castle, J. Čechal, B. M. Clark, H. Cohen, J. Counsell, A. Herrera-Gomez, P. Govindan, S. H. Kim, D. J. Morgan, R. L. Opila, C. J. Powell, S. Průša, A. Roberts, M. Rocca, N. Shirahata, T. Šikola, E. F. Smith, R. C. So, J. E. Stovall, J. Strunk, A. Teplyakov, J. Terry, S. G. Weber, and M. R. Linford, Perspective on improving the quality of surface and material data analysis in the scientific literature with a focus on x-ray photoelectron spectroscopy (XPS), *Journal of Vacuum Science & Technology A* **41**, 100534 (2023).

[3] D. Briggs and M. P. Seah, eds., *Practical Surface Analysis. Vol. 1: Auger and X-ray Photoelectron Spectroscopy* (John Wiley & Sons, Chichester, UK, 1990) p. 674.

[4] D. Briggs and J. Grant, eds., *Surface analysis by Auger and X-ray photoelectron spectroscopy* (IM Publications and SurfaceSpectra Limited, Trowbridge, UK, 2003).

[5] G. Greczynski and L. Hultman, A step-by-step guide to perform x-ray photoelectron spectroscopy, *Journal of Applied Physics* **132**, 011101 (2022).

[6] G. Greczynski, R. T. Haasch, N. Hellgren, E. Lewin, and L. Hultman, X-ray photoelectron spectroscopy of thin films, *Nature Reviews Methods Primers* **3**, 40 (2023).

[7] D. R. Baer, G. E. McGuire, K. Artyushkova, C. D. Easton, M. H. Engelhard, and A. G. Shard, Introduction to topical collection: Reproducibility challenges and solutions with a focus on guides to XPS analysis, *Journal of Vacuum Science & Technology A* **39**, 021601 (2021).

[8] J. W. Pinder, G. H. Major, D. R. Baer, J. Terry, J. E. Whitten, J. Čechal, J. D. Crossman, A. J. Lizarbe, S. Jafari, C. D. Easton, J. Baltrusaitis, M. A. van Spronsen, and M. R. Linford, Avoiding common errors in X-ray photoelectron spectroscopy

data collection and analysis, and properly reporting instrument parameters, *Applied Surface Science Advances* **19**, 100534 (2024).

[9] C. J. Powell, Practical guide for inelastic mean free paths, effective attenuation lengths, mean escape depths, and information depths in x-ray photoelectron spectroscopy, *Journal of Vacuum Science & Technology A: Vacuum, Surfaces, and Films* **38**, 023209 (2020).

[10] G. Greczynski and L. Hultman, Binding energy referencing in X-ray photoelectron spectroscopy, *Nature Reviews Materials* **10**, 62 (2024).

[11] D. R. Baer, K. Artyushkova, H. Cohen, C. D. Easton, M. Engelhard, T. R. Gengenbach, G. Greczynski, P. Mack, D. J. Morgan, and A. Roberts, XPS guide: Charge neutralization and binding energy referencing for insulating samples, *Journal of Vacuum Science & Technology A* **38**, 031204 (2020).

[12] V. B. Crist, XPS guide for insulators: Electron flood gun operation and optimization, surface charging, controlled charging, differential charging, useful FWHMs, problems and solutions, and advice, *Journal of Vacuum Science & Technology A* **42**, 032803 (2024).

[13] F. A. Stevie and C. L. Donley, Introduction to x-ray photoelectron spectroscopy, *Journal of Vacuum Science & Technology A* **38**, 063204 (2020).

[14] P. S. Bagus, C. J. Nelin, and C. R. Brundle, Chemical significance of x-ray photoelectron spectroscopy binding energy shifts: A Perspective, *Journal of Vacuum Science & Technology A* **41**, 068501 (2023).

[15] D. R. Baer and A. G. Shard, Role of consistent terminology in XPS reproducibility, *Journal of Vacuum Science & Technology A* **38**, 031203 (2020).

[16] H. Idriss, On the wrong assignment of the XPS O1s signal at 531–532 eV attributed to oxygen vacancies in photo- and electro-catalysts for water splitting and other materials applications, *Surface Science* **712**, 121894 (2021).

[17] C. D. Easton and D. J. Morgan, Critical examination of the use of x-ray photoelectron spectroscopy (XPS) O 1s to characterize oxygen vacancies in catalytic materials and beyond, *Journal of Vacuum Science & Technology A* **43**, 053205 (2025).

[18] M. C. Biesinger, Accessing the robustness of adventitious carbon for charge referencing (correction) purposes in XPS analysis: Insights from a multi-user facility data review, *Applied Surface Science* **597**, 153681 (2022).

[19] G. Greczynski, Binding energy referencing in X-ray photoelectron spectroscopy: Expanded data set confirms that adventitious carbon aligns to the sample vacuum level, *Applied Surface Science* **670**, 160666 (2024).

[20] G. H. Major, N. Fairley, P. M. A. Sherwood, M. R. Linford, J. Terry, V. Fernandez, and K. Artyushkova, Practical guide for curve fitting in x-ray photoelectron spectroscopy, *Journal of Vacuum Science & Technology A* **38**, 061203 (2020).

[21] P. M. Sherwood, The use and misuse of curve fitting in the analysis of core X-ray photoelectron spectroscopic data, *Surface and Interface Analysis* **51**, 589 (2019).

[22] V. Jain, M. C. Biesinger, and M. R. Linford, The Gaussian-Lorentzian Sum, Product, and Convolution (Voigt) functions in the context of peak fitting X-ray photoelectron spectroscopy (XPS) narrow scans, *Applied Surface Science* **447**, 548 (2018).

[23] M. O. Krause and J. H. Oliver, Natural widths of atomic K and L levels, K α X-ray lines and several K L L Auger lines, *Journal of Physical and Chemical Reference Data* **8**, 329 (1979).

[24] G. H. Major, T. G. Avval, D. I. Patel, D. Shah, T. Roychowdhury, A. J. Barlow, P. J. Pigram, M. Greiner, V. Fernandez, A. Herrera-Gomez, and M. R. Linford, A discussion of approaches for fitting asymmetric signals in X-ray photoelectron spectroscopy (XPS), noting the importance of Voigt-like peak shapes, *Surface and Interface Analysis* **53**, 689 (2021).

[25] J. Kockläuner, M. Shaker, M. Muth, S. Steinbach, C. Oleszak, O. Lytken, H.-P. Steinrück, and D. Golze, Decoding Shake-up Satellites in XPS through Large-Scale ab initio Simulations: Spectral Signatures of Ring Fusion in Porphyrins, *arXiv* , 2509.26057v1 (2025), arXiv:2509.26057.

[26] J. A. Gardella, S. A. Ferguson, and R. L. Chin, $\pi^* \leftarrow \pi$ Shakeup Satellites for the Analysis of Structure and Bonding in Aromatic Polymers by X-Ray Photoelectron Spectroscopy, *Applied Spectroscopy* **40**, 224 (1986).

[27] C. R. Brundle and B. V. Crist, X-ray photoelectron spectroscopy: A perspective on quantitation accuracy for composition analysis of homogeneous materials, *Journal of Vacuum Science & Technology A* **38**, 041001 (2020).

[28] D. A. Shirley, Many-electron and final-state effects: Beyond the one-electron picture, in *Photoemission in Solids I. Topics in Applied Physics, vol 26.*, edited by M. Cardona and L. Ley (Springer Berlin Heidelberg, 1978) pp. 165–195.

[29] A. E. Hughes, C. D. Easton, P. R. Anusuyadevi, T. J. Raeber, N. C. Wilson, and A. Mol, Widespread erroneous analysis of the Fe 2p peak in X-ray photoelectron spectroscopy examination in corrosion studies, *Corrosion Science* **257**, 113357 (2025).

[30] G. Moretti, Auger parameter and Wagner plot in the characterization of chemical states by X-ray photoelectron spectroscopy: a review, *Journal of Electron Spectroscopy and Related Phenomena* **95**, 95 (1998).

[31] D. R. Baer, M. T. Camci, D. J. H. Cant, S. A. Chambers, H. Cohen, P. Aydogan Gokturk, D. J. Morgan, A. Shchukarev, P. M. A. Sherwood, S. Suzer, S. Tougaard, and J. F. Watts, What more can be done with XPS? Highly informative but underused approaches to XPS data collection and analysis, *Journal of Vacuum Science & Technology A* **43**, 040801 (2025).

[32] S. Tougaard, Practical guide to the use of backgrounds in quantitative XPS, *Journal of Vacuum Science & Technology A* **39**, 011201 (2021).

[33] A. Jablonski, Emission depth distribution function for photoelectrons emitted by laboratory hard X-ray radiation sources, *Journal of Electron Spectroscopy and Related Phenomena* **195**, 26 (2014).

[34] M. H. Engelhard, D. R. Baer, A. Herrera-Gomez, and P. M. A. Sherwood, Introductory guide to backgrounds in XPS spectra and their impact on determining peak intensities, *Journal of Vacuum Science & Technology A* **38**, 063203 (2020).

[35] A. G. Shard, Practical guides for x-ray photoelectron spectroscopy: Quantitative XPS, *Journal of Vacuum Science & Technology A* **38**, 10.1116/1.5141395 (2020).

[36] A. Herrera-Gomez, D. M. Guzman-Bucio, M. Mayorga-Garay, and O. Cortazar-Martinez,

Angle resolved x-ray photoelectron spectroscopy assessment of the structure and composition of nanofilms—including uncertainties—through the multilayer model, *Journal of Vacuum Science & Technology A* **41**, 063206 (2023).

[37] A. G. Shard and M. A. Baker, Practical guides for x-ray photoelectron spectroscopy: Use of argon ion beams for sputter depth profiling and cleaning, *Journal of Vacuum Science & Technology A* **42**, 050801 (2024).

[38] S. A. Chambers, P. V. Sushko, and P. S. Bagus, Revisiting the assignment of atomic charges in metal oxides based on core-level x-ray photoelectron spectra: The case of Ti in SrTiO₃(001), *Journal of Vacuum Science & Technology A* **43**, 023203 (2025).